

Modern control for the secondary mirror of a Giant Segmented Mirror Telescope

Whorton M.^{1a}, Angeli, G.^{2b}

^aNASA Marshall Space Flight Center / Tennessee State University; ^bAURA New Initiatives Office

ABSTRACT

To achieve diffraction-limited seeing with the next generation of giant telescopes will require a multi-tiered approach employing both active and adaptive optics. Before removing atmospheric effects via adaptive optics, the telescope structure must be actively controlled to remove structural dynamics effects from the optical wavefront. While low frequency thermal and gravitational effects may be removed by the primary mirror control system, a more difficult challenge is the higher frequency, wind-induced vibrations of the telescope structure. This paper will address the control system design for the rigid secondary mirror support structure using modern control methods. Multivariable control methods are motivated by the large number of coupled structural modes that contribute to the wavefront error at the secondary mirror. H_2 methods are applied to the secondary mirror control system in order to validate the design approach for achieving nominal performance at the system level. The approach investigated for this paper involves using wavefront information to remove wavefront error at the secondary mirror. This work will serve as a basis for demonstrating the feasibility of the overall control architecture for the GSMT point design study.

Keywords: Flexible structures, optimal control, modern control, H_2 control, active optics, secondary mirror.

1. INTRODUCTION

Over the past two decades, significant advances have been made in vibration control technology for flexible structures. Much of this work was motivated by proposed civil and military space systems such as large solar collectors, deployed boom structures for x-ray astronomy, long-baseline interferometers, and space-based lasers. Common to each of these applications was the need to maintain precise pointing or positioning of a distributed, flexible structure. Space-based applications were more stringent than ground-based applications, in general, because high launch costs necessitated light and flexible space structures. Flexible space structures characteristically have numerous low frequency vibration modes that are closely spaced and lightly damped. The need for high control bandwidth to meet performance requirements combined with the low frequency structural modes poses quite a challenge for control system design. In large part, modern control technology has been developed to meet that challenge.¹

1.1 Motivation for Modern Control Technology

Classical control methods are based on a transfer function describing the response of a single output variable to a single input to the system. Although known to provide inherent robustness and simplicity of design and implementation, classical control methods are not well suited for multivariable (coupled) systems. Modern control is a term used for the class of multivariable linear control methods that operate on state space descriptions of a dynamic system. Many applications exist where the effect of an input or set of inputs cannot be decoupled in the system outputs. Of necessity, the control designer must often consider this cross-channel input-output coupling in the design and analysis of the control system. To do that requires a different set of design and analysis tools than does the single-input, single-output classical control design theory.

¹ mark.whorton@msfc.nasa.gov; phone 256-544-1435; NASA Marshall Space Flight Center, TD55/Control Systems, Huntsville, AL, USA 35812 (NASA Administrator's Fellow at The Tennessee State University, Center of Excellence in Information Systems, Nashville, TN).

² gangeli@gemini.edu; phone 520-318-8413; AURA New Initiatives Office, 950 N. Cherry Ave., Tucson, AZ, USA 85719.

Flexible structures are inherently multivariable systems. Disturbance forces and torques as well as control forces and torques affect multiple performance variables and sensed parameters. Although a state-space description of the input-output dynamics can be realized in a set of basis vectors that effectively decouples the system dynamics (such as the normal mode form), this decoupling is a function of the dynamic properties of the system such as mass and stiffness, or equivalently, the normal mode shapes and frequencies (eigenvectors and eigenvalues). These quantities are typically uncertain to some degree. When the uncertainties associated with mode shapes and frequencies correspond to the vibration modes within the control bandwidth, the potential for deleterious behavior is significant. This control/structure interaction can result from either low frequency modes or high control bandwidth. In either case, the structural modes encompassed by the control bandwidth must be well known to avoid the potential for degraded performance or instability. Modern control technology provides a means to explicitly account for multivariable coupling while considering both performance and robustness with respect to uncertainties.

2. MODERN CONTROL FOR GIANT TELESCOPES

Telescope assemblies with apertures on the order of 5-meters and smaller are typically constructed very rigidly to mitigate vibratory motion of the optics assembly. But things get more dynamic with larger apertures. Active control technology enabled two key developments leading to the class of 8-10 meter apertures telescopes. Active optics provided figure maintenance in the presence of thermal and gravity induced deformations while adaptive optics enabled diffraction limited seeing by removing atmospheric induced aberrations. These two control applications were decoupled: adaptive optics worked at high frequencies to locally control a small mass while active optics applied to large masses (for segmented or large deformable optics) at very low frequencies.

Moving to the realm of giant telescopes likewise requires more advanced control technology methods. Whereas the 8-10 meter telescopes exhibit structural dynamics effects that must be controlled, the issue becomes more pronounced with giant telescopes. Much like space structures, giant ground telescopes must be designed with mass constraints that lead to low frequency vibration modes. As an example, consider Table 1, which compares the structural dynamics of the 8-meter Gemini Telescope² with data from the 30-meter Giant Segmented Mirror Telescope (GSMT) Finite Element Model³. The Gemini telescope exhibits potential for telescope-induced aberrations, having six lightly damped modes below ten Hz. However, the GSMT structural dynamics are more pronounced, having twenty modes below ten Hz (with an assumed 2% damping in the model). Exacerbating the effect with giant telescopes are the turbulent wind forces that are likely to have a more pronounced disturbance effect with giant telescopes. As a result, active optics for giant telescopes must bridge the gap between the quasi-steady figure maintenance of the primary mirror and the high frequency adaptive optics of the instrumentation. Giant telescope control systems will require compensation for telescope induced vibratory aberrations in the optical wavefront. Due to the highly coupled and uncertain nature of the structural dynamics within the control bandwidth, modern control methods must be brought to bear.

2.1 Control Design Methods

Modern control methods provide a means to determine a feedback gain matrix that optimizes some aspect of the overall system description. Different methods produce different results based on the mathematical basis for the controller optimization. For the control designs in this paper, the generalized plant of a multi-input, multi-output system may be written in state space form as

$$\begin{aligned}\dot{x} &= A_p x + B_{1p} w + B_{2p} u \\ z &= C_{1p} x + D_{12p} u \\ y &= C_{2p} x + D_{21p} w + D_{22p} u\end{aligned}\tag{1}$$

where generically, $x \in \mathfrak{R}^n$ is the state vector, $w \in \mathfrak{R}^{nw}$ is the vector of disturbance inputs (such as wind forces), $u \in \mathfrak{R}^{nu}$ is the vector of control forces, $z \in \mathfrak{R}^{nz}$ is the vector of performance variables (those that are to be penalized in the control action), and $y \in \mathfrak{R}^{ny}$ is the measurement vector. Two standard modern control methods are H_2 and H_∞ control.⁴ The H_2 optimization problem is to find a stabilizing controller that minimizes the H_2 norm of the closed loop system from

disturbance inputs w to performance outputs z , denoted T_{zw} . Likewise, the H_∞ optimization problem is to find a stabilizing controller that minimizes the H_∞ norm of the closed loop system T_{zw} .

H_2 methods minimize an integral square quantity and as such are often used when designing control systems to reduce the vibration response of a flexible structure. While H_2 design gives good nominal performance, the controllers are highly tuned to the design model and errors in the design model are not accounted for, typically inducing instability at higher levels of control authority. As a result, the actual performance achievable is limited with H_2 designs. To achieve high levels of performance in the presence of uncertainties associated with the wind disturbances and structural dynamics, robustness must be taken into account in the design process.

Another approach to design for nominal performance employs the H_∞ norm, which can be interpreted as the gain of the system and is the worst-case amplification over all inputs $w(t)$ of unit energy. From a frequency domain perspective, the H_∞ norm is defined as the maximum singular value of $T(s)$ over all frequencies. Because the H_∞ norm is defined with respect to the peak magnitude of the transfer matrix frequency response and the H_2 norm is defined by an integral square quantity (in time or frequency by Parseval's Theorem), the respective closed loop systems typically have considerably different characteristics. Depending on the performance objectives, one design procedure may be preferable to the other. With regard to mean-square performance specifications such as minimizing the energy in a signal such as optical path difference, H_2 design is typically better suited for nominal performance. The significant benefit of H_∞ theory however is that robustness to uncertainties is explicitly factored into the design process.

Table 1: Structural Mode Comparison Between Gemini and GSMT

Mode #	Gemini Freq (Hz)	Damping (%)	Mode #	GSMT Freq (Hz)	Damping (%)
1	1.82	2.12	1	0.50	2
2	3.24	1.14	2	0.50	2
3	4.13	0.25	3	0.50	2
4	7.08	0.10	4	0.50	2
5	7.74	0.49	5	0.50	2
6	8.88	1.36	6	2.17	2
			7	2.49	2
			8	3.14	2
			9	4.00	2
			10	4.11	2
			11	4.26	2
			12	4.46	2
			13	5.05	2
			14	5.40	2
			15	6.66	2
			16	7.61	2
			17	8.09	2
			18	8.34	2
			19	8.81	2
			20	9.75	2

2.2 Limitations and Considerations

Modern control methods are indeed useful tools for challenging control applications such as giant telescopes and space structures. However, the benefits come with a price. A few of these issues will be mentioned here to put the task in context, but it is beyond the scope of this paper to address the nuances of these issues and detail the approaches to resolve them. Suffice it to say that the current state of the art in modern control theory addresses these issues.

Many of the limitations of modern control methods result from basing the control design on a model of the system. To achieve high performance in the implementation of these controllers requires a high fidelity model for design and/or analysis. The degree to which the model is uncertain is the degree to which robustness must be factored into the design process. Since robustness to uncertainties and performance of the control system are mutually opposed, the importance of an accurate model for the final design is imperative. Fortunately, modern control methods can optimize for performance in the presence of structured uncertainties in a fairly non-conservative manner.⁵⁻⁷ The ultimate performance is still limited by the degree of uncertainty in the model, which will always be significant for large structural systems.

Another issue common to modern control methods is the large dimension of the controller state vector. Methods for which a closed form analytical solution exist result in a controller with a state vector the same order as the generalized plant for control design, which often contains additional states for weighting functions and input/output scaling. Controller dimension is an important implementation issue that is constrained by the computer throughput capabilities. Methods exist for reducing the order of the controller, but closed loop performance and stability are often sacrificed. Better, so-called "fixed-order" methods directly impose constraints on the controller order in the optimization process so that the optimal controller of a fixed order is designed. These methods often nearly fully recover the full-order system characteristics, but the design process is extremely computationally intensive and not readily amenable to iterative design processes.¹

Since the objective of this paper is to validate the control architecture for the GSMT point design, these implementation issues will not be addressed in this work. In order to demonstrate the nominal performance achievable with this control architecture, H_2 control design will be applied. To demonstrate robustness to model uncertainties using H_∞ methods and fixed-order control methods would be merely academic at this point in the GSMT design process, especially since the applicability of these methods have been demonstrated by the author on related flexible structure control problems.⁸ These issues will be addressed with the appropriate methodology as the GSMT design matures and the implementation stage approaches.

3. SECONDARY MIRROR SUPPORT CONTROL DESIGN

The objectives of the GSMT point design are to explore a plausible design solution while identifying key technology issues and analytical methodology that must be addressed in order to meet the science goals for a 30-meter class telescope. Toward that end, a radio telescope configuration has been developed that incorporates an adaptive secondary mirror supported on a tripod structure as illustrated in Figure 1. The deformable facesheet of the secondary mirror is mounted to a rigid support structure which itself is actively controlled with five degrees of freedom. It is the control of this rigid body secondary mirror support to which this paper is directed. As discussed in the introduction, it is the need to remove optical aberrations induced by low frequency telescope vibration modes prior to removing atmospheric aberrations that distinguishes giant telescope control systems from previous generations of telescope controllers. Essentially this rigid support structure is a steering mirror used to remove wavefront error resulting from telescope-induced aberrations.

3.1 GSMT Structure and Optics Model

The GSMT finite element model was modified for this control design task to accommodate an independently controllable secondary mirror support. The secondary support structure was attached to the tripod support nodes through a compliant interface allowing five degrees of freedom relative motion between the secondary mirror support and the tripod attach points. Control and reaction forces are applied at this interface as well. This rigid mass and compliant interface added five modes at 0.5 Hz to the GSMT structure (the first five modes in Table 1 are due to the secondary mirror support degrees of freedom).

The objective of the overall GSMT control design is to produce the best possible image in the presence of atmospheric turbulence, wind buffeting, and telescope structural dynamics. Toward this end, the controller optimization objective is to minimize the spatial variance squared of the OPD, σ^2 , which in turn maximizes the Strehl ratio, S , of the image. (For

more specific details on the optical modeling for control design, see Reference 3 and the appendices therein). The optical path difference, \mathbf{p} , a function of position throughout the aperture, is a good measure of the image quality of the telescope and – for reasonably small deformations - a linear function of the mechanical displacements of the telescope structure. An OPD function defined on a circular aperture can be expanded into a discrete Zernike spectrum

$$b_j = \int_{\text{aperture}} Z_j(\mathbf{r})p(\mathbf{r})d\mathbf{r} = \sum_n^{aperture} Z_j(n)p(n) = \mathbf{w}_j \mathbf{p}$$

where Z_j is the j^{th} Zernike term evaluated at position \mathbf{r} or node n and b_j is the corresponding coefficient. The Strehl ratio is related to the spatial variance of the OPD as:

$$S = e^{-\left(\frac{2\sigma}{\lambda}\right)^2}$$

To maximize the Strehl ratio, the spatial variance of the OPD should be minimized. An approximation of the spatial variance of the OPD can be computed from the selected Zernike coefficients of the OPD as follows:

$$\hat{\sigma}^2 = \sum_{i=1}^N a_i^2$$

Using a linear combination of the Zernike coefficients of the subsystem deformations (\mathbf{b}) and the corresponding sensitivity matrices (\mathbf{S}), the Zernike coefficients of the OPD (\mathbf{a}) are determined from

$$\mathbf{a}_{\text{system}} = \mathbf{a}_{\text{atmosphere}} + \mathbf{S}_{\text{primary}} \mathbf{b}_{\text{primary}} + \mathbf{S}_{\text{secondary}} \mathbf{b}_{\text{secondary}}$$

where the \mathbf{b} terms are computed from the structural displacements of the primary and secondary mirror. Thus at each time step, the Zernike coefficients of the primary and secondary mirror deformations are computed, from which the Zernike expansion of the OPD is computed by virtue of the optical sensitivity matrices.

3.2 Control Design Description

H_2 control methods are well suited to this GSMT application because they minimize an integral square output quantity for white noise disturbance input (shaped in the plant by disturbance filters). From Parseval's theorem, the H_2 norm is equivalent in both the time and frequency domain. So, the time domain system (state space) can be used to optimize the integral of the OPD variance square (which is a spatial frequency term).

Figure 2 presents the control architecture enforced to decouple the control in terms of both temporal frequency and Zernike modes of the optical path difference (OPD)⁹. Based on this architecture, the secondary support structure controller must remove the lowest order wavefront error in the DC - 10 Hz bandwidth that is too large for the adaptive optics to accommodate. Wavefront sensor measurements provide tip and tilt (Zernike modes 1 and 2) feedback to the active control system, which applies three forces and two torques to the rigid secondary support structure. The primary disturbances in this frequency range arise from wind loading on the secondary and primary mirrors. In addition to the direct wind loads, the unsteady aerodynamics of the turbulent vortices shed across the primary mirror face excites the low frequency vibration modes of the telescope structure.¹⁰ For control design, wind loads with a white noise spectral content are applied to both the primary mirror and the secondary mirror.

Representative, measured wind profiles are applied for the control system evaluation.¹¹ In the particular case used for simulation, the telescope is pointing into the wind with zenith angle of 30°. The average wind velocity at both the primary and secondary mirror is about 4 m/s with horizontal direction.

The first 20 modes of the GSMT were retained in the 40 state control design model. Input wind forces were applied to the GSMT telescope structure in three axes at a representative node on the tripod and in one axis at three representative

nodes on the primary mirror. The wind loads to the primary mirror were only applied in the direction normal to the mirror surface. Figure 3 presents the block diagram of the generalized plant for H_2 control design.

For the H_2 control designs, the control weight, ρ , ranged from 0.1 to 0.00001 to vary control authority. As the penalty on control decreases in the cost function (for optimal control design), the controller is allowed to more actively respond to the measurements and is thus said to have higher authority. With reference to Figure 3, the disturbance inputs include the aforementioned wind forces and tip-tilt sensor noise. The measurement vector consists of the tip and tilt measurements of the wavefront (OPD). Likewise, the performance variables are defined as the weighted tip and tilt error (the first two Zernike modes of the OPD) and the weighted control, z_u . Note that the tip and tilt errors are computed from the structural deformations of the primary mirror and the tripod using an optical sensitivity matrix. (A parameter need not be measured or even physically meaningful to serve as a performance variable, it simply must be mathematically constructed as an output of the plant model.) Controllers were designed using the first eight Zernike modes as performance variables, but the performance did not noticeably differ from the control designs which only penalized the first two modes.

3.3 Control Design Results

A set of controllers with varying control authority was designed, resulting in H_2 controllers with 40 states. Figure 4 shows the nominal performance design results for the H_2 control designs as the control authority is varied. As the control authority increases, greater attenuation of the wavefront error is observed. Performance for the multivariable system here is presented in terms of the maximum singular value of the system with input wind disturbances and the first two Zernike modes of the OPD as the output. The maximum singular value represents an upper bound on the system gain at each frequency -- essentially a worst-case input and output gain for the set of inputs and outputs. The controller represented by the lowest curve (e.g. the greatest OPD attenuation) is used for the following performance evaluation.

Whereas a relatively low order model with a small number of wind disturbance inputs was used for control design, the controller performance evaluation was performed with a higher fidelity model and more representative wind load profiles. A 100 mode (200 state) model of the GSMT dynamics is used with 91 wind input nodes on the primary and six nodes on the tripod vertex. Normal forces were applied to the primary mirror nodes and three orthogonal forces were applied to each tripod node. A representative wind profile sampled at 40 Hz for 300 seconds was used for the time history simulation.

For each time response, a Zernike expansion of the structural deformations at the primary and secondary mirror locations was computed. The Zernike coefficients of the OPD were then expressed as a linear combination of the Zernike coefficients of the deformations, resulting in a time response of the first eight Zernike modes of the image wavefront passing through the telescope.¹¹ From these open and closed loop time responses, power spectral densities (PSD) were computed for the first eight Zernike modes of the OPD. Figures 5 through 8 present the PSD of the open and closed loop Zernike terms for modes 1,2,6, and 7, corresponding to x tilt, y tilt, 0° coma and 90° coma, respectively. These figures demonstrate the significant improvement in x and y tilt achieved by controlling the secondary mirror. Note that this control has a minimal improvement on the 0° coma and a slight degradation for 90° coma.

The validation of this design architecture is demonstrated in Figures 9 and 10. Figure 9 presents a PSD of the spatial RMS of the OPD that indicates the significant attenuation of wavefront error at the low frequencies achieved by controlling the rigid body secondary support motion. This spatial RMS was computed at each time instant of the wind response simulation. From this time history of the Spatial RMS of the OPD, a PSD was computed and then integrated backwards in frequency to give the cumulative RMS above a particular frequency. This "residual RMS" is plotted in Figure 10. In other words, at each frequency, the value on the plot in Figure 10 is the temporal RMS of the spatial RMS for wind response above that frequency (e.g. the integral of the PSD of the spatial RMS OPD time history above that frequency). Figure 10 indicates that the total RMS spatial error is reduced from approximately 40 microns to around 5 microns above 10 Hz while above 10 Hz, the open loop RMS spatial error is reduced from 2 microns to approximately 0.3 microns. Assuming that the primary mirror control system adequately provides figure maintenance, these results show that a controller using tip and tilt measurements at the secondary mirror sufficiently removes the wavefront error

introduced by telescope vibrations. The residual RMS of the wavefront error can adequately be removed by the adaptive optics systems.

4. CONCLUSIONS

The validation of the decoupling design architecture for the GSMT has been demonstrated by implementing an H_2 controller for the secondary mirror support structure. Because of the inherent coupling through structural dynamics, modern multivariable control methods are deemed especially appropriate for the secondary mirror support structure. Using feedback of the tip and tilt at the secondary mirror, five degrees of freedom are controlled to mitigate wavefront aberrations induced by telescope structural dynamics. Future work will address implementation issues such as controller order and robustness to model uncertainties.

ACKNOWLEDGEMENTS

This work was funded by the New Initiatives Office, which is a partnership between two divisions of the Association of Universities for Research in Astronomy (AURA), Inc.: the National Optical Astronomy Observatory (NOAO) and the Gemini Observatory.

NOAO is operated by AURA under cooperative agreement with the National Science Foundation (NSF).

The Gemini Observatory is operated by AURA under a cooperative agreement with the NSF on behalf of the Gemini partnership: the National Science Foundation (United States), the Particle Physics and Astronomy Research Council (United Kingdom), the National Research Council (Canada), CONICYT (Chile), the Australian Research Council (Australia), CNPq (Brazil) and CONICET (Argentina).

REFERENCES

1. M. Whorton, "High Performance, Robust Control of Flexible Space Structures," Ph.D. Thesis, The Georgia Institute of Technology, September 1997.
2. D. Smith, "Gemini South 8m Optical Telescope Final Report, MACL Report # 05-08570-001," Modal Analysis and Controls Laboratory, Mechanical Engineering Department, University of Massachusetts at Lowell, Lowell, Massachusetts, October 2000.
3. "Enabling a Giant Segmented Mirror Telescope for the Astronomical Community" <http://www.auranio.noao.edu/book/index.html>
4. J. Maciejowski, *Multivariable Feedback Design*, Addison Wesley, 1989.
5. J. Doyle, "Analysis of feedback systems with structured uncertainties," Proc. IEE-D 129, 1982, pp 242-250.
6. J. Doyle, "Lecture Notes on Advances in Multivariable Control," ONR/Honeywell Workshop on Advances in Multivariable Control, Minneapolis, MN, October, 1984.
7. J. Doyle, C. Chu, "Robust Control of Multivariable and Large Scale Systems," Final Technical Report for AFOSR, Contract No. F49620-84-C-0088, March 1986.
8. M. Whorton, A. Calise, C. Hsu, "A Study of Fixed Order Mixed Norm Designs for a Benchmark Problem in Structural Control," *Earthquake Engineering and Structural Dynamics*, No. 27, pp. 1315-1330, 1998
9. G. Angeli, M. Cho, B. Gregory, M. Whorton, "Active Optics and Control Architecture for a Giant Segmented Mirror Telescope," SPIE Astronomical Telescopes and Instrumentation Conference, Waikoloa, HI, August 22-28, 2002.

10. G. Xu, M. Whorton, Y. Tao, M. Cho, "Dynamic Modeling of Turbulent Shedding Effect on the 30-meter Primary Mirror of GSMT," SPIE Astronomical Telescopes and Instrumentation Conference, Waikoloa, HI, August 22-28, 2002.

11. M. K. Cho, L. Stepp, S. Kim, "Wind buffeting effects on the Gemini 8m primary mirror" *Proceedings of SPIE* **4444**, 302-314 (2001)

12. G. Angeli, "Linear Optical Model for a Cassegrain Telescope (GSMT)," NIO-TNT-006, AURA New Initiatives Office, May 30, 2002.

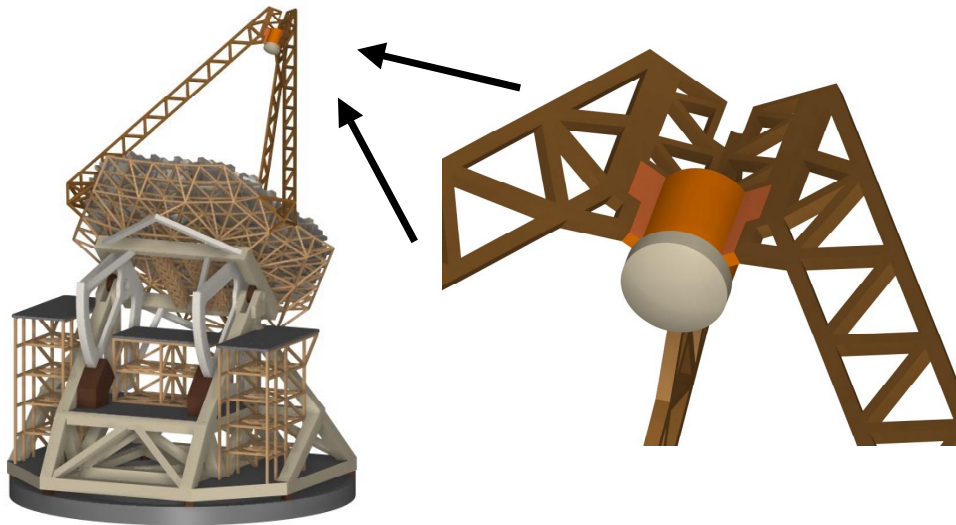


Figure 1: GSMT Structure with Secondary Mirror Detail

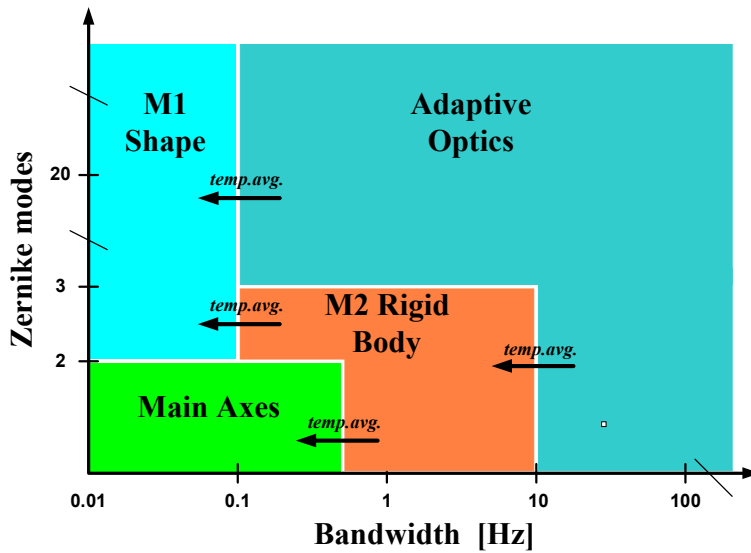


Figure 2: GSMT Control Architecture

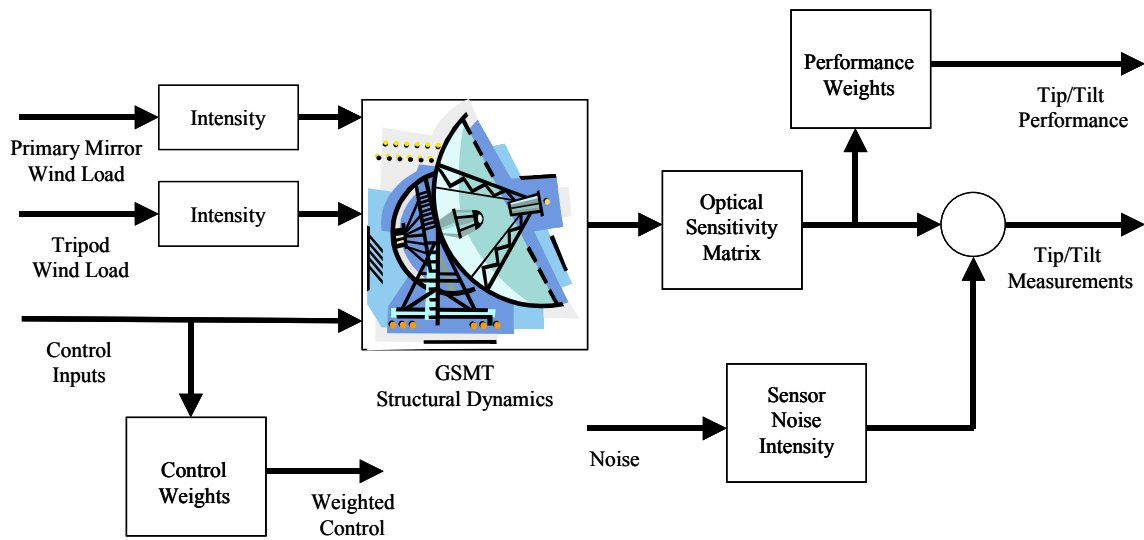


Figure 3: Generalized Plant for H₂ Control Design

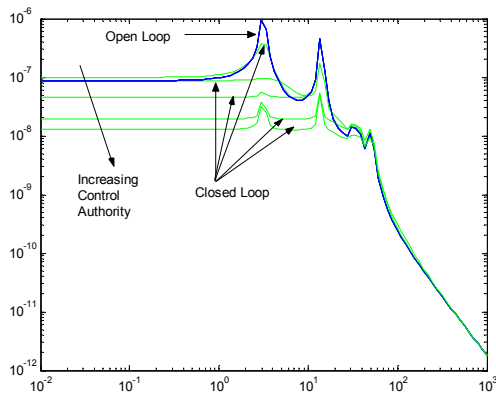


Figure 4: Open Loop and Closed Loop Maximum Singular Values for Wind Load Disturbance to Tip and Tilt Wavefront Error

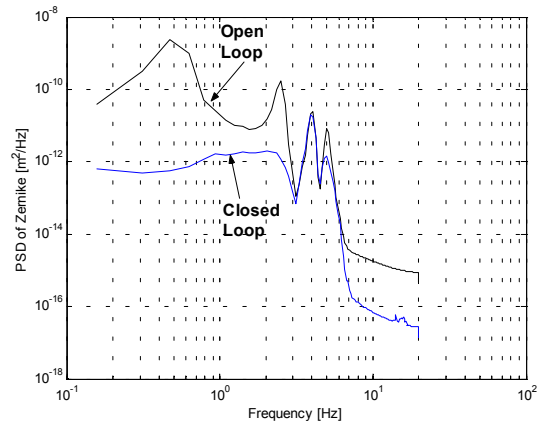


Figure 5: Open Loop and Closed Loop PSD of Zernike Term #1 (X-Tip) of Image Aberration (Total OPD)

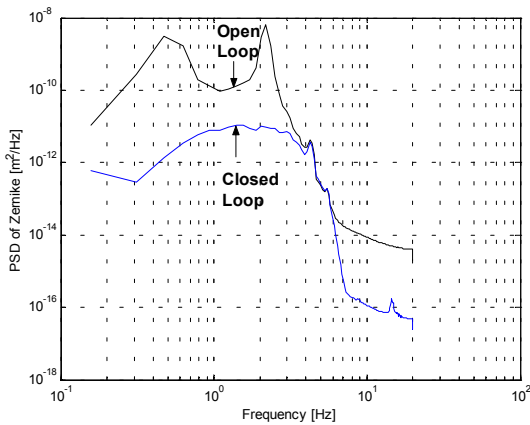


Figure 6: Open Loop and Closed Loop PSD of Zernike Term #2 (Y-Tilt) of Image Aberration (Total OPD)

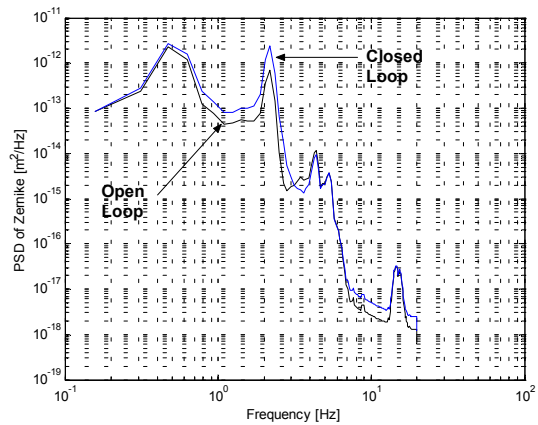


Figure 8: Open Loop and Closed Loop PSD of Zernike Term #7 (90° Coma) of Image Aberration (Total OPD)

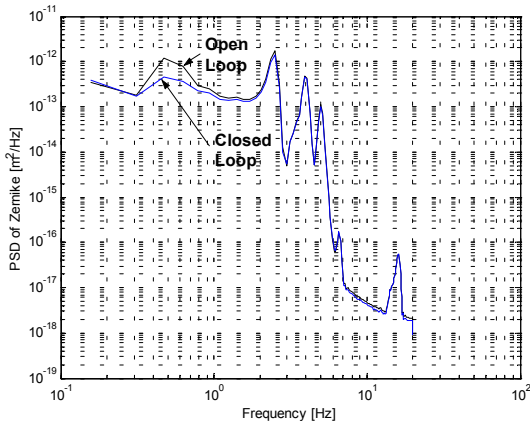


Figure 7: Open Loop and Closed Loop PSD of Zernike Term #6 (0° Coma) of Image Aberration (Total OPD)

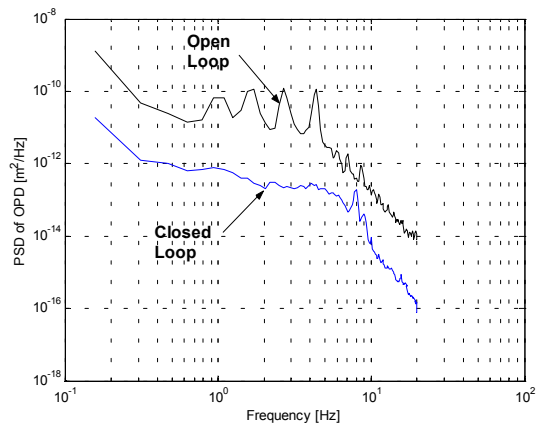


Fig. 9: Open Loop and Closed Loop Power Spectral Density of the Spatial RMS of Image Aberration (Total OPD)

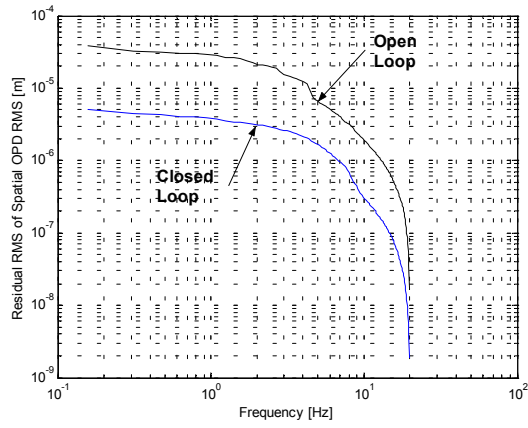


Fig. 10: Open Loop and Closed Loop (H2) Residual RMS of the Spatial RMS of Image Aberration (Total OPD)